2020 IEEE/RSJ International Conference on Intelligent Robots and Systems (IROS)
October 25-29, 2020, Las Vegas, NV, USA (Virtual)

An Optimized Tilt Mechanism for a New Steady-Hand Eye Robot

Jiahao Wu, Gang Li, Muller Urias, Niravkumar A. Patel, Yun-hui Liu, Peter Gehlbach, Russell H. Taylor, and Iulian Iordachita

***Abstract*— Robot-assisted vitreoretinal surgery can filter surgeons' hand tremors and provide safe, accurate tool manipulation. In this paper, we report the design, optimization, and evaluation of a novel tilt mechanism for a new Steady-Hand Eye Robot (SHER). The new tilt mechanism features a four-bar linkage design and has a compact structure. Its kinematic configuration is optimized to minimize the required linear range of motion (LRM) for implementing a virtual remote center-of-motion (V-RCM) while tilting a surgical tool. Due to the different optimization constraints for the robots at the left and right sides of the human head, two configurations of this tilt mechanism are proposed. Experimental results show that the optimized tilt mechanism requires a significantly smaller LRM (e.g. 5.08 mm along Z direction and 8.77 mm along Y direction for left side robot) as compared to the slider-crank tilt mechanism used in the previous SHER (32.39 mm along Z direction and 21.10 mm along Y direction). The feasibility of the proposed tilt mechanism is verified in a mock bilateral robot-assisted vitreoretinal surgery. The ergonomically acceptable robot postures needed to access the surgical field is also determined.**

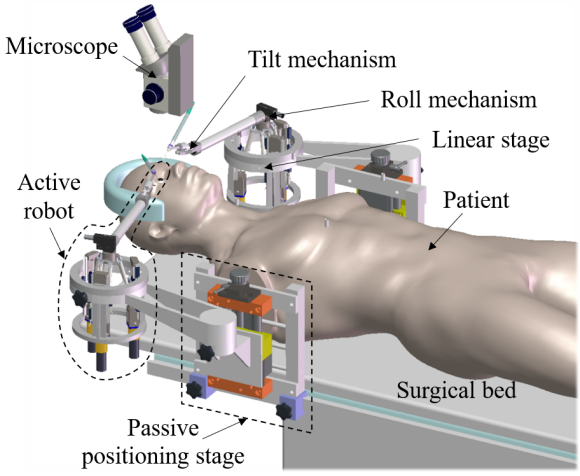

Fig. 1. Concept design of the new Steady-Hand Eye Robot.

I. Introduction

Vitreoretinal surgery is a challenge to be performed safely and efficiently largely due to: 1) the extremely small intraocular structures (e.g. the thickness of the retina is about 100-300 μm [1] and the diameter of the retinal vessel is smaller than 130 μm [2]); 2) physiological hand tremor (over 100 μm [3]). Robot-assisted vitreoretinal surgery has been shown to overcome these limitations and has attracted the attention of researchers and surgeons in recent years [4]. Teleoperated, handheld and cooperatively controlled robots are the three most representative robotic systems in this field.

Teleoperated robotic systems are implemented by a master-slave control approach. The first teleoperated robot proposed for ocular surgery was a stereotaxical microtelemanipulator (SMOS) [5]. This robot could manipulate a tool to within the eyeball through a sclera entry point. The remote center-of-motion (RCM) design of this robot allows the motion of the tool to pivot about the entry point to improve safety. Although the da Vinci robotic system has been used in conjunction with the hexapod surgical system to perform such surgical operations [6], the accuracy of the system cannot meet the surgical requirements. PRECEYES is the clinically-applied example of a robot of this class. It is composed of an XYZ linear stage and a four-degree-of-freedom (DOF) linkage-based RCM mechanism [7]. The advantages of the teleoperated robotic systems are reflected by three characteristics: 1) the use of master/slave motion scaling can achieve precise tool manipulation, 2) the hand tremor present on the master console can be filtered out from the slave, and 3) the robot has the ability to perform remote surgery. Among the disadvantages are the large footprint and complex design.

A handheld micromanipulator, Micron, has also been proposed to help surgeons filter unintentional motions, such as hand tremor, while maintaining direct manual control of the surgical instruments [8]. However, it cannot provide RCM due to its limited DOF. Therefore, a new version of Micron consisting of a 6-DOF piezoelectric Stewart parallel mechanism was developed [9]. Micron however can only preserve a 1:1 force feedback ratio, which is potentially unfavorable in vitreoretinal surgery.

A cooperative control approach, in which both the surgeon and the robot hold the surgical tool, has been proposed in [10]. The robot detects the force exerted by the surgeon on the instrument and moves accordingly. The advantages of this approach over other robotic systems include: 1) potential lower cost, 2) direct coupling to human natural motion sensation, and 3) easy integration into existing operating environments [10]. Two generations of the Steady-Hand Eye Robot were developed at the Johns Hopkins University and widely investigated in the artificial phantom and animal model experiments [11]–[13]. Various control methods with a series of force-sensing tools [14]–[17] were introduced into

This work was supported by U.S. National Institutes of Health under grant number 1R01EB025883-01A1. The work of J. Wu was supported in part by the HK RGC under T42-409/18-R and 14202918. (*Corresponding author: jhwu@mae.cuhk.edu.hk*)

J. Wu and Y.-H. Liu are with the T Stone Robotics Institute, the Department of Mechanical and Automation Engineering, The Chinese University of Hong Kong, HKSAR, China, and J. Wu is also with LCSR at the Johns Hopkins University, Baltimore, MD 21218 USA (email: jhwu, yhliu@mae.cuhk.edu.hk).

G. Li, N. Patel, R. Taylor, I. Iordachita are with LCSR at the Johns Hopkins University, Baltimore, MD 21218 USA (email: gli22, rht, iordachita@jhu.edu).

M. Urias, P. Gehlbach are with the Wilmer Eye Institute, Johns Hopkins Hospital, Baltimore, MD 21287 USA (e-mail: murias1, pgelbach@jhmi.edu).

the SHER to provide accurate, hand-tremor-free, and smooth tool operation.

The previous SHERs are still underqualified for clinical application due to several limitations, such as bulky serial linear stage, and inconvenient integration into the surgical environment, etc. Based on our prior work, we aim to develop the next generation Steady-Hand Eye Robot meeting the requirements of clinical application. The concept design of the new robotic system is illustrated in Figure 1. To achieve bilateral tool manipulation in a single eyeball, the system is composed of two 5-DOF active robots, each mounted on a 3-DOF passive positioning stage that is attached directly to the surgical bed. The two active robots are designed with almost identical mechanism and each is composed of a 3-DOF linear stage, a 1-DOF roll mechanism and a 1-DOF tilt mechanism.

The linear stage adopts a parallel delta mechanism [18], which can improve the accuracy and rigidity of the entire system as compared to the serial design used in the previous SHER. However, to keep the parallel mechanism compact, it tends to have a limited linear range of motion (LRM). In the cooperatively-controlled robot-assisted vitreoretinal surgery, the space near the surgical field is limited and the space for the surgeon's hand to hold the tool must be large enough to work efficiently and safely. Consequently, a compact design of the tilt mechanism is essential.

In this paper, a novel compact tilt mechanism adopting the four-bar linkage design is proposed. The RCM is taken into account of the design to enhance safety during operations. The kinematic configuration of the proposed tilt mechanism is optimized to minimize the required LRM of the linear stage for implementing a virtual RCM (V-RCM) while tilting a surgical tool. Due to the different optimization constraints for the robots at the left and right sides of the patient's head, two configurations of this tilt mechanism are proposed. The main contributions of this paper are summarized as follows:

- A novel optimized compact tilt mechanism for the new Steady-Hand Eye Robot is designed to minimize the required LRM of the linear stage for implementing a V-RCM;
- Two kinematic configurations of the tilt mechanism are proposed for the robots on different sides of the patient's head.
- A study with a retinal surgeon performing a mock vitreoretinal surgery is conducted to determine the ergonomically acceptable robot postures to access the surgical field.

The rest of the paper is organized as follows: In section II, we describe the design requirements of the tilt motion and present the optimization process and results of the proposed novel tilt mechanism. In section III, experiments are conducted to evaluate the performance and feasibility of the tilt mechanism. Conclusions and future work are presented in Section IV.

II. Design and Optimization of the Tilt Mechanism

A. Design Requirements

During vitreoretinal surgery, tools (e.g. light pipe, cannula, micro forceps, etc.) are inserted into an eyeball ($\phi 25\ mm$) through sclera entry points in order to reach the retina (see Fig. 2). The sclera entry point is defined approximately at $9\ mm$ away from the optical axis because there is no vital tissue at this location. 4-DOF motion is required to manipulate the tool inside the eyeball: the axial translation of the tool through the entry point and the spin, roll and tilt motion around the entry point. Based on our proposed concept design of the new robot, the axial translation can be realized through a coupled movement of the linear stage, the tool can spin freely in the tool holder, and the roll/tilt motions are realized using the roll/tilt mechanisms. To ensure the RCM, the linear stage offers motion compensation (i.e. required LRM) for the tool to tilt around the sclera entry point.

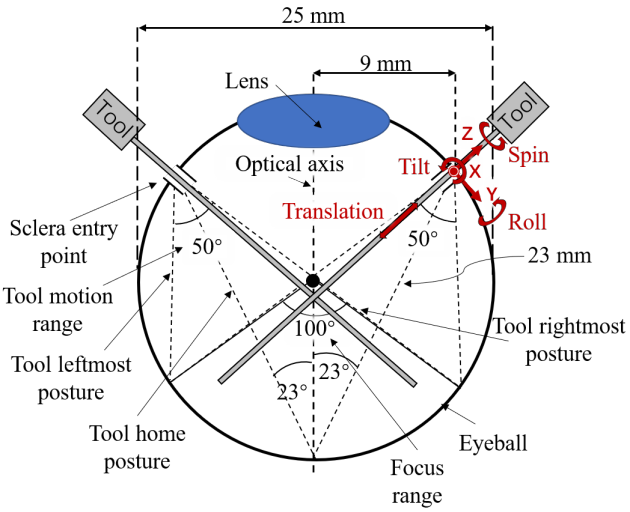

Fig. 2. Tool motion inside the eyeball for vitreoretinal surgery.

As mentioned in [19], during vitreoretinal surgery, the surgeon's focus range is the area on the retina of $60°$ around the center of the eyeball. The range is increased up to $100°$ to provide surgeons sufficient freedom to manipulate the tool during the operation (see Fig. 2). Given the above information, the necessary tilt motion range of the tool is calculated as $50°$. The home posture of the tool is defined as the posture where the tool points through the scleral entry point to the center of the bottom of the eyeball. The angle between the home posture and the optical axis is approximately $23°$. By rotating the tool from the home posture $25°$ clockwise and counterclockwise, we obtain the leftmost and rightmost postures.

In this article, we focus on the design of the tilt mechanism. As mentioned above, the design requirements include: 1) the mechanism should be capable of manipulating the tool from the leftmost position to the rightmost position of $50°$, 2) should be compact, and 3) requires small LRM for implementing a V-RCM.

B. Design Concept of the Tilt Mechanism

The RCM for the tool should be considered to enhance safety during operations. Researchers normally adopt the parallel six-bar mechanism (see Fig. 3(b)) to implement mechanical RCM (used in SHER 2 [12]). However, the complex and bulky structure of this design and the limited

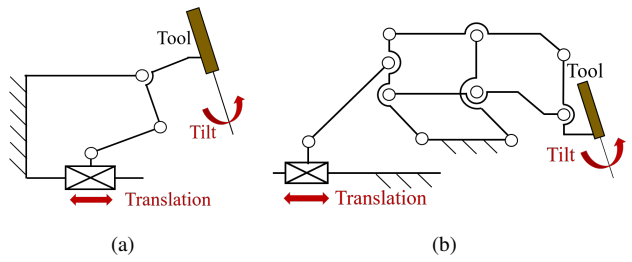

Fig. 3. Previous tilt mechanism used for SHER: (a) Slider-crank mechanism used for SHER 1; (b) Parallel six-bar mechanism used for SHER 2.

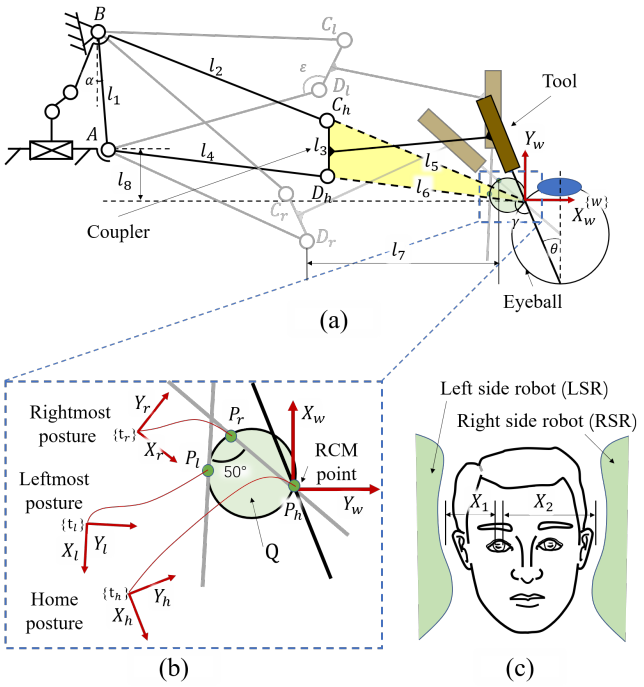

Fig. 4. (a) Design concept and parameters of the four-bar linkage tilt mechanism. (b) Three focused tool postures, i.e. rightmost, home, and leftmost postures. The smallest circle **Q** covering the RCM points of three postures is defined. (c) Safe distance between the robot and operation space.

hand-holding space lead to significant constraints for the cooperatively controlled robot. Another choice is to use the slider-crank mechanism (see Fig. 3(a)) to implement a virtual RCM (V-RCM) (used in SHER 1 [11]). This design is simple and compact but requires large LRM to implement a V-RCM. Using this design will lead to an undesirably larger delta robot of the new SHER.

Four-bar linkage is widely used in mechanical systems [20]. A link grounded by a hinged joint is usually called a crank, while a link that connects two cranks is called a coupler. Based on the mechanism synthesis, the rigid body attached to the coupler can have a series of prescribed postures.

Taking advantages of the aforementioned characteristics of the four-bar linkage mechanism, we propose the concept of the new tilt mechanism. As shown in Fig. 4(a), a tool is attached to the coupler of a four-bar linkage mechanism actuated by a slider-crank mechanism. This design is more compact than the parallel six-bar mechanism. To meet the required tilt angle range of the tool in vitreoretinal surgery, three prescribed postures of the tool is defined (i.e. leftmost, home, and rightmost postures as shown in Fig. 2). RCM point is defined as the point attached to the tool shaft that coincides with the sclera entry point at the home posture. Note that at other postures, RCM point of the tool is not coincident with the sclera point since our tilt mechanism is not true mechanical RCM design. To implement the V-RCM, the LRM provided by the linear stage makes the RCM point coinciding with the sceral entry point.

Proposed three postures are represented by X_iY_i frame $\{t_i\}$, whose origin P_i is attached to the RCM point and X_i axis is set along the tool shaft (see Fig. 4(b). In this paper, $i = l, h, r$ represent the proposed three tool postures, respectively. X_wY_w frame $\{w\}$ represents the world frame, whose origin is defined at the sclera entry point and Y axis is parallel to the optical axis.

To define the required LRM, the smallest circle **Q** (see Fig. 4(b)) covering the RCM points of three postures is used. Since the delta robot has limited LRM while keeping compact, an optimization approach is introduced to derive the kinematic configuration of the tilt mechanism while minimizing the size of the circle **Q**.

C. Optimization of the Tilt Mechanism

As shown in Fig. 4(a), A, B, C_i, and D_i represent the joints of the four-bar linkage. The length of the links are represented by l_1, l_2, l_3, and l_4, respectively. Since the tool is fixed on the coupler, the length l_5 of the link C_iP_i, the length l_6 of the link D_iP_i, and the angle γ between the link D_iP_i and the axis of the tool keep constant for $\forall\ i = l, h, r$. In addition, α represents the angle between link AB and vertical line, ϵ represents the angle between the links D_lC_l and D_lA, and l_7 represents the horizontal distance between points D_h and P_h. In this paper, distances, coordinates, and angles are expressed in mm and deg, respectively. The following are the detailed procedures to perform the optimization.

1) Optimization variables: There are eight variables that should be optimized as shown in follows:

$$[x_t^C, y_t^C, x_t^D, y_t^D, x_w^{P_l}, y_w^{P_l}, x_w^{P_r}, y_w^{P_r}], \tag{1}$$

where $[x_t^C, y_t^C]$ and $[x_t^D, y_t^D]$ are the coordinates of C_i and D_i expressed in the tool frame $\{t_i\}$, respectively. For $\forall\ i = l, h, r$, the above two coordinates keep constant. $[x_w^{P_l}, y_w^{P_l}]$ and $[x_w^{P_r}, y_w^{P_r}]$ are the coordinates of the RCM point P_l and P_r expressed in the world frame $\{w\}$. The lower and upper bounds of the variables are set as [-120, -120, -120, -120, -25, -25, -25, -25] and [20, 20, 20, 20, 25, 25, 25, 25] based on the consideration of the design requirements and computation efficiency.

2) Optimization objective: As previously mentioned, our aim is to minimize the size of the circle **Q** (i.e. required LRM) while tilting the tool from the leftmost posture to the rightmost posture. Therefore, the optimization objective for our case is set as follows:

$$\min\ r_Q, \tag{2}$$

where r_Q represents the radius of the smallest covering circle $\mathbf{Q}$ calculated as follows:

$$r_Q = \begin{cases} \frac{1}{2} max\{l_{P_l P_h}, l_{P_r P_h}, l_{P_l P_r}\}, & \text{if } \Delta P_l P_h P_r \text{ is an obtuse triangle,} \\ \sqrt{(x_w^{P_l} - x_w^Q)^2 + (y_w^{P_l} - y_w^Q)^2}, & \text{if } \Delta P_l P_h P_r \text{ is an acute/right triangle,} \end{cases} \tag{3}$$

where

$$\begin{aligned} l_{P_l P_h} &= \sqrt{(x_w^{P_l} - x_w^{P_h})^2 + (y_w^{P_l} - y_w^{P_h})^2}, \\ l_{P_r P_h} &= \sqrt{(x_w^{P_r} - x_w^{P_h})^2 + (y_w^{P_r} - y_w^{P_h})^2}, \\ l_{P_l P_r} &= \sqrt{(x_w^{P_l} - x_w^{P_r})^2 + (y_w^{P_l} - y_w^{P_r})^2}, \end{aligned} \tag{4}$$

$[x_w^{P_h}, y_w^{P_h}] = [0, 0]$ is the coordinate of P_h expressed in the world frame $\{w\}$, $[x_w^Q, y_w^Q]$ is the coordinate of the center of the circumscribed circle of points P_l, P_h, and P_r expressed in the world frame $\{w\}$.

3) Optimization constraints: In this work, only the following constraints are considered.

- To leave space for the force sensor installed between the coupler and the tool, as well as provide sufficient hand-holding space for the surgeon, we have:

$$\begin{aligned} &[40, 40] \leq [l_5, l_6] \leq [150, 150], \\ &60^\circ \leq \gamma \leq 150^\circ. \end{aligned} \tag{5}$$

where

$$\begin{aligned} l_5 &= \sqrt{(x_t^C)^2 + (y_t^C)^2}, \\ l_6 &= \sqrt{(x_t^D)^2 + (y_t^D)^2}, \\ \gamma &= cos^{-1}(\frac{x_t^D}{l_6}). \end{aligned} \tag{6}$$

- To leave space for the bearings at the joints and keep the tilt mechanism compact, we have:

$$[10, 10, 10, 10] \leq [l_1, l_2, l_3, l_4] \leq [100, 100, 100, 100], \tag{7}$$

where

$$\begin{aligned} l_1 &= \sqrt{(x_w^B - x_w^A)^2 + (y_w^B - y_w^A)^2}, \\ l_2 &= \sqrt{(x_w^B - x_w^{C_h})^2 + (y_w^B - y_w^{C_h})^2}, \\ l_3 &= \sqrt{(x_t^C - x_t^D)^2 + (y_t^C - y_t^D)^2}, \\ l_4 &= \sqrt{(x_w^A - x_w^{D_h})^2 + (y_w^A - y_w^{D_h})^2}, \end{aligned} \tag{8}$$

$[x_w^B, y_w^B]$ and $[x_w^A, y_w^A]$ are the coordinates of joints B and A expressed in the world frame $\{w\}$, respectively. The above two points locate at the center of the circumscribed circle of points C_l, C_h and C_r and the center of the circumscribed circle of points D_l, D_h and D_r, respectively. The coordinates of joints C_i and D_i expressed in the world frame $\{w\}$ are shown as follows:

$$\begin{aligned} [x_w^{C_i}, y_w^{C_i}]^T &= [x_w^{P_i}, y_w^{P_i}]^T + \boldsymbol{R}_w^{t_i} [x_t^C, y_t^C]^T, \\ [x_w^{D_i}, y_w^{D_i}]^T &= [x_w^{P_i}, y_w^{P_i}]^T + \boldsymbol{R}_w^{t_i} [x_t^D, y_t^D]^T, \end{aligned} \tag{9}$$

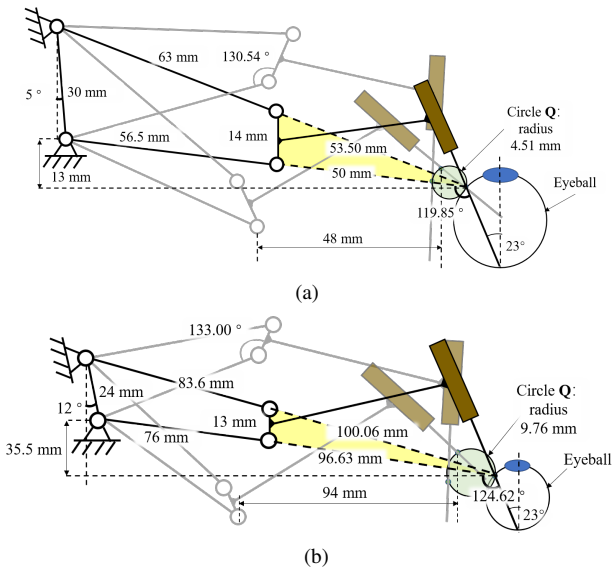

Fig. 5. Kinematic configurations. (a) Kinematic configurations of LSR; (b) Kinematic configurations of RSR;

where $i = l, h, r$, $\boldsymbol{R}_w^{t_i} \in \mathbb{R}^{2\times 2}$ is a rotation matrix that describes the orientation of the tool frame $\{t_i\}$ with respect to the world frame $\{w\}$. The rotation matrix can be derived due to the prescribed orientation of the tool frame $\{t_i\}$ (see Fig. 2 and Fig. 4(b)).

- To avoid approaching dead-center while tilting the tool, we have:

$$\epsilon = cos^{-1}(\frac{l_3^2 + l_4^2 - l_{AC_l}^2}{2 l_3 l_4}) < 160^\circ, \tag{10}$$

where $l_{AC_l} = \sqrt{(x_w^A - x_w^{C_l})^2 + (y_w^A - y_w^{C_l})^2}$ is the length of the link AC_l.

- To avoid robot collisions with the patient, joint D_r should keep a safe distance away from the point P_r. As shown in Fig.4(c), the left side robot (LSR) and the right side robot (RSR) have different safe distances. Based on our previous experience and [21], the safe distances X_1 and X_2 are set to $45\ mm$, and $94\ mm$, respectively. Therefore, we have:

$$l_7 = x_w^{P_r} - x_w^{D_r} \geq \begin{cases} 45, & \text{if LSR,} \\ 94, & \text{if RSR} \end{cases} \tag{11}$$

that is the key constraint that results in two different kinematic configurations for LSR and RSR.

4) Genetic algorithm: In this paper we use a modified genetic algorithm (GA) (multi-island GA) to implement the optimization based on Matlab and Isight. Each population individual is divided into several small groups called "islands" [22]. All traditional genetic operations are performed on each sub-population separately, then individuals are selected from each island and regularly migrated to different islands. Using the aforementioned multi-island GA, optimization variables can be effectively updated to minimize the objective function. The sub-population size is 10, the number of islands is 10, the number of generations is 100000,

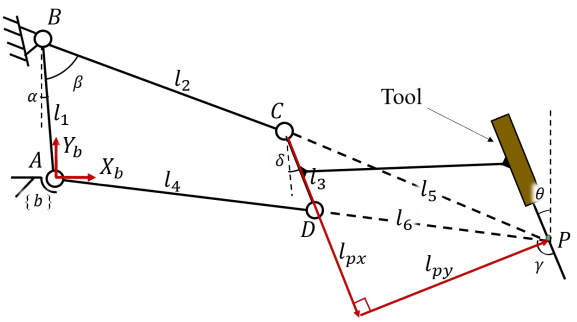

Fig. 6. Geometry of the four-bar linkage tilt mechanism.

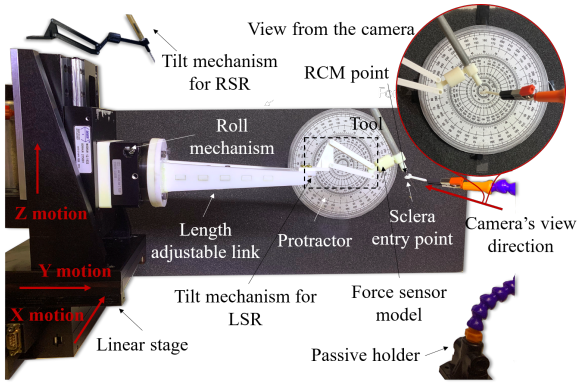

Fig. 7. Experimental setup of the required LRM evaluation.

the rate of crossover is 1.0, the rate of mutation is 0.01, and the rate of migration is 0.01.

5) Optimization results: In consideration of mechanical manufacturing, we have refined the results. The optimized variables (see (1)) are [-37.77, -37.89, -24.88, -43.37, -8.78, 1.77, -6.83, 5.07] for LSR, and [-66.86, -74.44, -54.90, -79.53, -19.07, 1.38, -16.45, 9.38] for RSR. The resulting kinematic configurations of the tilt mechanism are shown in Fig. 5. The radius of the circle **Q** is minimized to $4.52\ mm$ for LSR and $9.76\ mm$ for RSR. Note that these parameters are for the setup of right eye. For the left eye, the LSR and RSR should be swapped.

D. Kinematics of the Tilt Mechanism

The kinematics of the proposed tilt mechanism can be derived from the geometric constraints shown in Fig. 6. The base frame of the tilt mechanism is set at the joint A and the Y axis is parallel to the vertical axis. β represents the actuation angle of the tilt mechanism. The tilt angle θ and the coordinates of the RCM point P expressed in the base frame $\{b\}$ can represent the posture of the tool.

To calculate the aforementioned parameters, first we can define the positions of C, D, and P as follows:

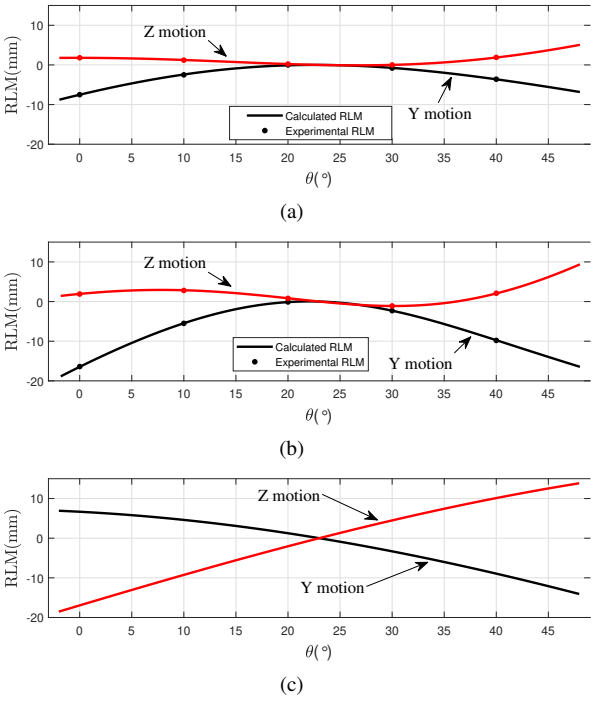

Fig. 8. RLM verification for (a) the proposed new tilt mechanism for LSR; (b) the proposed new tilt mechanism for RLR; (c) the slider-crank mechanism in SHER 1.

$$
\begin{aligned}
\boldsymbol{P}_b^C &= [x_b^C, y_b^C]^T \\
&= [-l_1 sin\alpha + l_2 sin(\alpha+\beta), l_1 cos\alpha - l_2 cos(\alpha+\beta)]^T, \\
\boldsymbol{P}_b^D &= [x_b^D, y_b^D]^T \\
&= \boldsymbol{P}_b^C + \begin{bmatrix} sin(\alpha+\delta) & cos(\alpha+\delta) \\ -cos(\alpha+\delta) & sin(\alpha+\delta) \end{bmatrix} \begin{bmatrix} l_3 \\ 0 \end{bmatrix}, \\
\boldsymbol{P}_b^P &= [x_b^P, y_b^P]^T \\
&= \boldsymbol{P}_b^C + \begin{bmatrix} sin(\alpha+\delta) & cos(\alpha+\delta) \\ -cos(\alpha+\delta) & sin(\alpha+\delta) \end{bmatrix} \begin{bmatrix} l_{px} \\ l_{py} \end{bmatrix},
\end{aligned} \tag{12}
$$

where

$$
\begin{aligned}
&\delta = cos^{-1}\left(\frac{l_3^2 - l_4^2 + d^2}{2 l_3 d}\right) - cos^{-1}\left(\frac{l_1 - l_2 cos\beta}{d}\right), \\
&d = \sqrt{l_1^2 + l_2^2 - 2 l_1 l_2 cos\beta}.
\end{aligned} \tag{13}
$$

Using the above formulas, the tilt angle θ can be calculated as follows:

$$
\theta = \gamma - 90^\circ - sin^{-1}\left(\frac{y_b^D - y_b^P}{l_6}\right). \tag{14}
$$

III. Experiments and Results

To validate the performance and feasibility of the proposed tilt mechanism, the prototypes of the optimized kinematic configurations were built using 3D printing approach. As an initial estimate based on surgical and mechanical requirements, the insertion depth (i.e. the distance between the tool tip and the RCM point) is set to 23 mm. The kinematic configurations of the mechanism for LSR and RSR are shown in Fig. 7. To mimic the real situation, we also add a cylinder

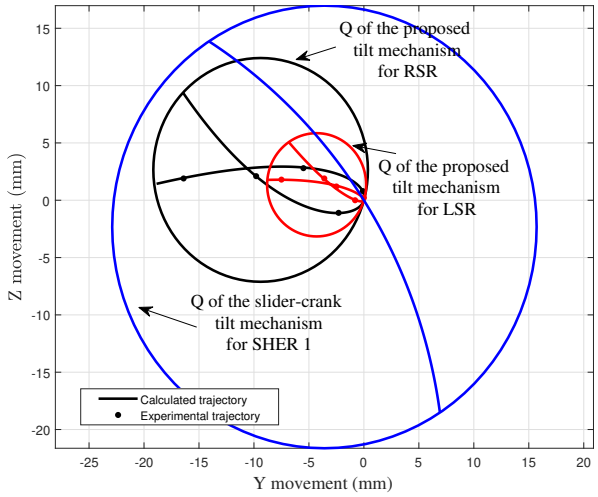

Fig. 9. Red, black and blue lines represent the RCM point trajectory of the proposed new tilt mechanism for LSR, RSR, and the slider-crank mechanism used in SHER 1, respectively.

between the coupler and the tool to indicate the force sensor (ATI Nano17, ATI Industrial Automation, NC). Each of the tilt mechanisms was then mounted on the roll mechanism of a 4-DOF robotic platform through a length adjustable link, which was built of laser cut Acrylic sheet (see Fig. 7).

The 3-DOF XYZ linear stage of the robot mimicked the 3-DOF linear delta mechanism in the new SHER design. The roll mechanism provided the roll motion for the tool. Those 4-DOF can be actuated through the interface of SHER and can also be manually driven. The position of those 4-DOF can be recorded using the built-in encoders and can also be manually recorded. For simplicity, we drove and recorded manually and the tilt motion of the prototype was passive.

A. Required LRM Evaluation

This experiment was conducted to verify the required LRM for the new tilt mechanism to implement the V-RCM. As shown in Fig. 7, a protractor was placed behind the tilt mechanism and was perpendicular to the ground and parallel to the Y direction of the linear stage. A camera was mounted on the front of the robot to record the motion. From the camera's view, the sclera entry point (represented by a plastic ring) coincided with the center of the protractor. The RCM point attached to the tool was marked in black.

The tilt mechanism was rotated through a set of angles varying from -25° to $+25^\circ$ with respect to the home posture (see Fig. 2). The roll mechanism was fixed at 0°. The linear stage was driven to ensure that the RCM point on the tool was coincident with the sclera entry point. The required linear movements (RLM) along Y and Z direction of the stage were recorded.

The calculated RLM from the formulas in section II-D and the experimental RLM are shown in Fig. 8. Both the RLM along Z motion and Y motion of the linear stage are shown. Fig. 8(a) indicates the RLM of the proposed new tilt mechanism for LSR are: $-0.01\ mm \sim 5.07\ mm$ along the Z direction, $-8.77\ mm \sim 0\ mm$ along the Y direction. The proposed tilt mechanism for RSR requires a LRM of $5.08\ mm$ along the Z direction, and $8.77\ mm$ along Y the direction. Similarly, as shown in Fig. 8(b), for the tilt mechanism for RSR, the required LRM along the Z direction is $10.50\ mm$. and along the Y direction is $18.90\ mm$. To compare with the slider-crank tilt mechanism used for SHER 1, we calculated the RLM for this design as shown in Fig. 8(c). The required LRM along the Z direction is $32.39\ mm$. and along the Y direction is $21.10\ mm$. Fig. 9 plots these trajectories of the RCM point of the tool while tilting about 50°. According to the above analysis, the optimzied four-bar linkage tilt mechanism can significantly reduce the required LRM for implementing a V-RCM.

B. Study of the Mock Robot-Assisted Vitreoretinal Surgery

To further verify the feasibility of the proposed tilting mechanism, a study of vitreoretinal surgery was performed using an adult manikin model. An experienced retinal surgeon participated in this experiment. The setup for the study is shown in Fig. 10. The robot arm accessed the surgical field from the left side and right side of the manikin head to hold the surgical tool. For each side, the robot entered in three different orientations ($+30^\circ$, 0°, and -30° with respect to the horizontal, respectively). Exploration of the phantom using this setup showed that in the $\pm 25^\circ$ tilt range from the home posture, the surgeon was comfortably able to collaborate with the robot, had sufficient tool holding space and the robot was able to avoid collision with the manikin's head during the operation.

The surgeon also gave feedback following the experience for each accessing case. During case 1 and 4, the surgeon's hand gesture was similar to the free-hand operation, but the robot arm affected the movement of the surgeon's arm. At case 3 and 6, the hand posture was considered awkward. Moreover, in case 6, the robot arm entered from the top of the nose which was uncomfortable for the surgeon. Compared to the aforementioned cases, case 2 and 5 were the more ergonomically acceptable robot postures for the surgeon to conduct the surgical tasks.

IV. Conclusions and Future Work

In this paper, we proposed the design, optimization, and evaluation of a novel tilt mechanism. This tilt mechanism adopted a four-bar linkage design that had a compact structure. Its kinematic configuration was optimized to minimize the required LRM for implementing a V-RCM. Two configurations of this mechanism were optimized for LSR and RSR, respectively. The required LRM evaluation experiments showed that the optimized tilt mechanism required a significantly smaller LRM as compared to the conventional slider-crank tilt mechanism. The study of the mock vitreoretinal surgery verified the feasibility of the new tilt mechanism to be used for bilateral tool manipulation and indicated that the 0° robot entering angle from the horizontal was ergonomically acceptable for the surgeon.

In the future, using the proposed kinematic configurations, we will conduct a detailed design to enhance the mechanical stiffness of the tilt mechanism, and build the complete new SHER. The proposed tilt mechanism has the potential to be adopted by other surgical robots that need both a compact robotic structure and a RCM constraint, such as Ear Nose and Throat (ENT) surgical robot.

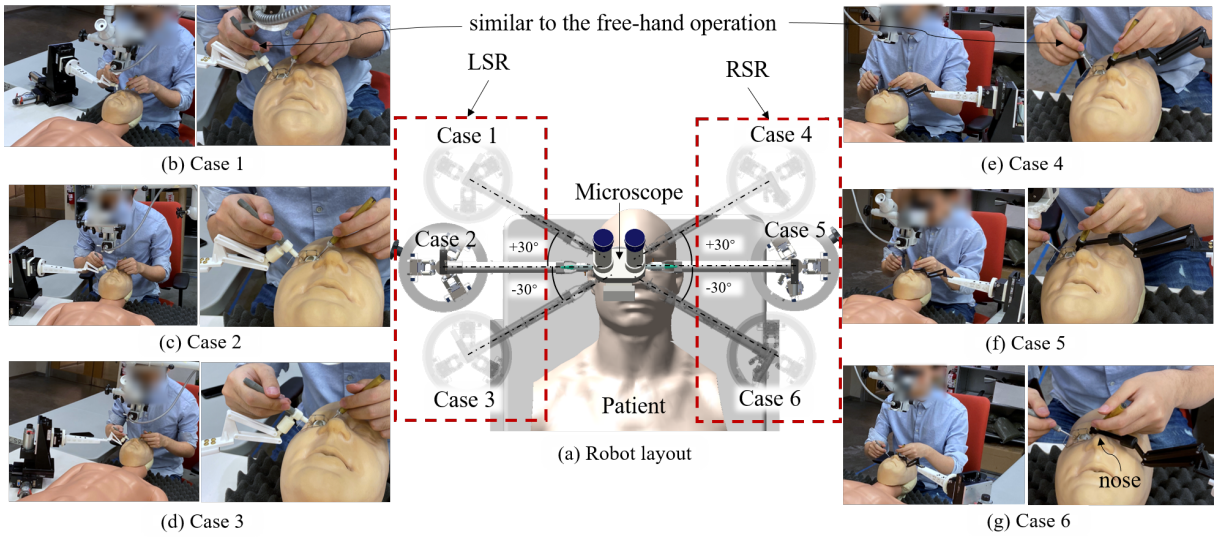

Fig. 10. Study of the mock robot-assisted vitreoretinal surgery including the cases that robot accesses the surgical field from the left side at (a) $+30^\circ$, (b) 0°, (c) -30° from the horizontal, with respect to the right side at (d) $+30^\circ$, (e) 0°, (f) and -30° with respect to the horizontal, respectively.

REFERENCES

[1] T. Leng, J. M. Miller, K. V. Bilbao, D. V. Palanker, P. Huie, and M. S. Blumenkranz, "The chick chorioallantoic membrane as a model tissue for surgical retinal research and simulation," *Retina*, vol. 24, no. 3, pp. 427–434, 2004.

[2] T. Rim, Y. Choi, S. Kim, M. Kang, J. Oh, S. Park, and S. Byeon, "Retinal vessel structure measurement using spectral-domain optical coherence tomography," *Eye*, vol. 30, no. 1, p. 111, 2016.

[3] S. Singh and C. Riviere, "Physiological tremor amplitude during retinal microsurgery," in *Proceedings of the IEEE 28th Annual Northeast Bioengineering Conference (IEEE Cat. No. 02CH37342)*. IEEE, 2002, pp. 171–172.

[4] E. Vander Poorten, C. N. Riviere, J. J. Abbott, C. Bergeles, M. A. Nasseri, J. U. Kang, R. Sznitman, K. Faridpooya, and I. Iordachita, "Robotic retinal surgery," in *Handbook of Robotic and Image-Guided Surgery*. Elsevier, 2020, pp. 627–672.

[5] A. Guerrouad and M. Bengayed, "An advanced control micromanipulator for surgical applications," *International system sciences*, 1986.

[6] J.-L. Bourges, J.-P. Hubschman, J. Wilson, S. Prince, T.-C. Tsao, and S. Schwartz, "Assessment of a hexapod surgical system for robotic micro-macro manipulations in ocular surgery," *Ophthalmic research*, vol. 46, no. 1, pp. 25–30, 2011.

[7] P. Gomes, *Medical robotics: Minimally invasive surgery*. Elsevier, 2012.

[8] R. A. MacLachlan, B. C. Becker, J. C. Tabarés, G. W. Podnar, L. A. Lobes Jr, and C. N. Riviere, "Micron: an actively stabilized handheld tool for microsurgery," *IEEE Transactions on Robotics*, vol. 28, no. 1, pp. 195–212, 2011.

[9] S. Yang, R. A. MacLachlan, and C. N. Riviere, "Manipulator design and operation of a six-degree-of-freedom handheld tremor-canceling microsurgical instrument," *IEEE/ASME transactions on mechatronics*, vol. 20, no. 2, pp. 761–772, 2014.

[10] R. Taylor, P. Jensen, L. Whitcomb, A. Barnes, R. Kumar, D. Stoianovici, P. Gupta, Z. Wang, E. Dejuan, and L. Kavoussi, "A steady-hand robotic system for microsurgical augmentation," *The International Journal of Robotics Research*, vol. 18, no. 12, pp. 1201–1210, 1999.

[11] B. Mitchell, J. Koo, I. Iordachita, P. Kazanzides, A. Kapoor, J. Handa, G. Hager, and R. Taylor, "Development and application of a new steady-hand manipulator for retinal surgery," in *Proceedings 2007 IEEE International Conference on Robotics and Automation*. IEEE, 2007, pp. 623–629.

[12] A. Üneri, M. A. Balicki, J. Handa, P. Gehlbach, R. H. Taylor, and I. Iordachita, "New steady-hand eye robot with micro-force sensing for vitreoretinal surgery," in *2010 3rd IEEE RAS & EMBS International Conference on Biomedical Robotics and Biomechatronics*. IEEE, 2010, pp. 814–819.

[13] X. He, D. Roppenecker, D. Gierlach, M. Balicki, K. Olds, P. Gehlbach, J. Handa, R. Taylor, and I. Iordachita, "Toward clinically applicable steady-hand eye robot for vitreoretinal surgery," in *ASME 2012 international mechanical engineering congress and exposition*. American Society of Mechanical Engineers Digital Collection, 2012, pp. 145–153.

[14] I. Iordachita, Z. Sun, M. Balicki, J. U. Kang, S. J. Phee, J. Handa, P. Gehlbach, and R. Taylor, "A sub-millimetric, 0.25 mn resolution fully integrated fiber-optic force-sensing tool for retinal microsurgery," *International journal of computer assisted radiology and surgery*, vol. 4, no. 4, pp. 383–390, 2009.

[15] C. He, E. Yang, and I. Iordachita, "Dual-stiffness force-sensing cannulation tool for retinal microsurgery," in *2019 41st Annual International Conference of the IEEE Engineering in Medicine and Biology Society (EMBC)*. IEEE, 2019, pp. 3212–3216.

[16] C. He, N. Patel, M. Shahbazi, Y. Yang, P. L. Gehlbach, M. Kobilarov, and I. Iordachita, "Toward safe retinal microsurgery: development and evaluation of an rnn-based active interventional control framework," *IEEE Transactions on Biomedical Engineering*, 2019.

[17] J. Wu, C. He, M. Zhou, A. Ebrahimi, M. Urias, N. Patel, Y.-h. Liu, P. Gehlbach, and I. Iordachita, "Force-based safe vein cannulation in robot-assisted retinal surgery: a preliminary study," *IEEE International Symposium on Medical Robotics (ISMR)*, 2020.

[18] F. Pierrot, C. Reynaud, and A. Fournier, "Delta: a simple and efficient parallel robot," *Robotica*, vol. 8, no. 2, pp. 105–109, 1990.

[19] A. Gijbels, N. Wouters, P. Stalmans, H. Van Brussel, D. Reynaerts, and E. Vander Poorten, "Design and realisation of a novel robotic manipulator for retinal surgery," in *2013 IEEE/RSJ International Conference on Intelligent Robots and Systems*. IEEE, 2013, pp. 3598–3603.

[20] A. G. Erdman and G. N. Sandor, *Mechanism design analysis and synthesis (Vol. 1)*. Prentice-Hall, Inc., 1997.

[21] "U.s. department of defense human factors engineering technical advisory group," *Human eng. design data digest*, p. 72–75, 2000.

[22] D. Whitley, S. Rana, and R. B. Heckendorn, "The island model genetic algorithm: On separability, population size and convergence," *Journal of computing and information technology*, vol. 7, no. 1, pp. 33–47, 1999.